Plasmonics (2016) 11:1369–1376
DOI 10.1007/s11468-016-0186-5

Correlating Metal-Enhanced Fluorescence and Structural Properties in $Ag@SiO_2$ Core-Shell Nanoparticles

Jérémie Asselin[1] · **Philippe Legros**[1] · **Alexandre Grégoire**[1] · **Denis Boudreau**[1]

Received: 4 December 2015 / Accepted: 2 March 2016 / Published online: 12 March 2016

Abstract Metal@silica concentric nanoparticles capable of metal-enhanced fluorescence (MEF) represent a powerful means to improve the brightness and stability of encapsulated organic fluorophores and are finding numerous applications in biology, analytical chemistry, and medical diagnostics. The rational design of MEF-enabled labels and sensors often involves comparing fluorescence enhancement factors (EF) between nanostructures having different structural properties (e.g., metal core diameter, silica shell thickness, extent of spectral overlap between plasmon band and fluorophore). Accurate determination of EFs requires the measurement of fluorescence emission intensity in the presence and absence of the plasmonic core while minimizing the impact of physical and chemical artifacts (e.g., signal variations due to scattering, adsorption, sedimentation). In this work, $Ag@SiO_2@SiO_2+x$ (where x is fluorescein, eosin, or rhodamine B) nanostructures were synthesized with excellent control of core size, silica spacer shell thickness and fluorophore concentration. Using UV-VIS spectrometry, spectrofluorimetry, time-resolved fluorometry, and transmission electron microscopy, we investigated the influence of these key structural factors on fluorescence emission intensity, and the results were used to develop a generalized methodology for the determination of fluorescence enhancement factors in $Ag@SiO_2$ core-shell nanoparticles. This methodology should be of general importance to designing MEF-enabled nanostructures, sensors, and related analytical techniques.

Keywords Plasmonics · Hybrid nanostructures · Metal nanoparticles · Plasmon-enhanced fluorescence · Metal-enhanced fluorescence

Introduction

Sensitive detection of chemical species using fluorescence has become massively popular in analytical and biological sciences, particularly in cellular and molecular imaging, flow cytometry, medical diagnostics, DNA sequencing, forensics, and genetic analysis [1–6]. Unfortunately, the intrinsically high sensitivity of fluorimetry may be compromised by the limited brightness, excitation cross-section, and photostability of many common molecular probes, leading to unsatisfactory detection limits or excessively long observation times. Several years ago, pioneering work by several groups sought to overcome these limitations by exploiting the interaction between the electrons responsible for surface plasmon resonance in metal nanoparticles and nearby fluorophores [7–13]. By combining the amplification of the incident electric field at or near the surface of nanoparticles and the coupling of excited fluorophores with the electrons in the particles, they succeeded in enhancing excitation and emission rates several-fold, while shortened excited state lifetimes improved robustness towards photobleaching [14]. This process was termed metal-enhanced fluorescence (MEF) to distinguish it from surface-enhanced fluorescence (SEF), which mainly concerns the enhancement of the incident field near metallic surfaces without necessarily involving dipole-dipole coupling between the metal surface and the fluorophore [15]. Other names for this phenomenon include plasmon-controlled

Electronic supplementary material The online version of this article (doi:10.1007/s11468-016-0186-5) contains supplementary material, which is available to authorized users.

✉ Denis Boudreau
denis.boudreau@chm.ulaval.ca

[1] Département de chimie et Centre d'optique photonique et laser (COPL), Université Laval, Québec, QC G1V 0A6, Canada

fluorescence (PCF) [16] or shell-isolated nanoparticle-enhanced fluorescence (SHINEF) [17]. Today MEF is being investigated as a powerful means to enhance the optical properties of commercially available luminescent dyes and to increase the detection sensitivity of various biological assays and imaging techniques [18–21].

Numerous studies performed using, for example, molecular assemblies over silver island films (SIF) deposited on glass slides [22–24], nanostructured planar systems fabricated with lithographic or ion beam methodologies [25, 26] and single-molecule studies [13, 25, 27] have shown that maximizing MEF for a given nanostructure-fluorophore system hinges on the optimization of several factors, notably the size, shape and chemical composition of the nanoparticles [27–31], the distance between metal nanoparticles and the fluorescent molecule(s) or between adjacent nanoparticles [23, 24, 32, 33] and the degree of overlap between the plasmon band and the fluorescence excitation-emission spectrum [34]. Unfortunately, the complexity of such precisely engineered nanofabricated plasmonic substrates tends to limit their use in biosensing applications, in particular where one needs to probe the interior of cells or extended sample volumes and for which freely diffusing nanostructures are often preferred [20, 35].

In comparison, a *core-shell* geometry where the nanostructure is in the form of a discrete metal nanoparticle separated from an outer fluorescent layer by a silica spacer shell (or other suitable dielectric material) retains all the advantages provided by MEF, including enhanced brightness and photostability, while being highly dispersible in aqueous media and easily conjugated to target biomolecules [36, 37]. Several studies have been published in recent years on the influence on fluorescence enhancement or quenching of structural parameters such as core shape and size, spacer shell thickness, and spectral overlap [23, 31, 38–40] and have led to a better understanding of structure-property relationships in MEF-enabled core-shell systems. However, because the colloidal synthesis methods generally used to fabricate core-shell nanoparticles do not provide the same level of geometrical control as state-of-the-art lithographic techniques, most studies examining the effects of structural parameters have been fragmented across different nanostructure types/compositions or limited to certain sizes or particular fluorophores. Therefore, a generalized model or methodology was not available to help determine the extent of MEF in multilayer core-shell nanoparticles. Fortunately, significant progress was made recently towards the synthesis of various multilayer core-shell metallic colloids, not only with silver or gold [41–43], but also more reactive elements like indium [30], aluminum [44], and copper [45], with excellent control over nanoparticle geometry, crystallinity, size uniformity, and shell thickness.

In the work presented herein, we have performed a detailed structure-property study in MEF-capable core-shell nanoparticles, using a seed-growth synthesis technique and rigid silica shells as spacers to precisely control the diameter of silver cores and the distance between the core surface and a thin layer of fluorescent silica on the outer surface of the nanostructures. Nanoparticles with nominal core diameters of 30, 40, 60, and 75 nm and spacer shell thicknesses from ~3 to >25 nm were prepared and coated with a ~1-nm outer silica layer doped with different fluorophores (fluorescein, eosin, and rhodamine B isothiocyanates) chosen for their varying degree of spectral overlap with the metal core plasmon band. The core-shell nanostructures were examined by transmission electron microscopy (TEM) and their concentration in each sample was determined by elemental analysis, and this information was used to determine the concentration of fluorescent molecules immobilized in the outer shell of each nanoparticle formulation. Their spectral properties were characterized by UV-VIS spectrometry, steady-state and time-resolved fluorimetry. Finally, fluorescence enhancement factors were determined and compared as a function of core size, spacer shell thickness, and spectral overlap.

Experimental Details

Chemicals and Reagents

Sodium citrate tribasic dihydrate (≥99.0 %, ACS grade), fluorescein 5(6)-isothiocyanate (FiTC; 90 %), rhodamine B isothiocyanate (RBiTC; mixed isomers), triethylamine (≥99.5 %), (3-aminopropyl)triethoxysilane (APTES; ≥98 %), ammonium hydroxide solution (28–30 % NH_3), dimethylamine (DMA; 40 %wt solution in water), sodium borohydride (99.99 %), and silver nitrate (≥99.0 %) were purchased from Sigma-Aldrich. High purity silver nitrate (99.9995 %) was obtained from Strem Chemicals, eosin-5-isothiocyanate (EiTC) from Marker Gene Technologies, tetraethoxysilane (TEOS; 99.9 %) from Alfa Aesar, and anhydrous *N*,*N*-dimethylformamide (DMF; 99.8 %) from EMD Chemicals. Unless otherwise stated, every chemical reagent was used without further purification. Nanopure water (18 MΩ) was used in all experiments and anhydrous ethanol (Commercial Alcohols, Brampton, ON, Canada) was used as a solvent. All glassware for nanoparticles synthesis was conditioned with concentrated nitric acid and rinsed thoroughly with water.

Preparation of Ag Nanoparticles by Seed-Growth

The silver cores were prepared by a seed-growth procedure using silver seeds as a starting material to grow larger nanoparticles. This methodology was adapted from various other sources [46–48] and provides precise control over core diameter from ~20 to more than 100 nm, with good repeatability with regards to polydispersity and plasmonic properties. In the present study, nanoparticles with well-controlled and uniform sizes (nominal diameters of 30, 40, 60, and 75 nm) were

prepared using a succession of growth steps. In a 250-mL round bottom flask, 75 mL of nanopure water was heated to 70 °C under vigorous stirring, 20 mL of 1 %wt aqueous sodium citrate (34 mM) was added and the temperature was allowed to stabilize for 10 min. 1.7 mL of 1 %wt aqueous $AgNO_3$ (59 mM, purity 99.0 %) and 0.2 mL of freshly made 1 %wt aqueous $NaBH_4$ (264 mM) were then quickly added to the sodium citrate solution and the mixture was left to stir for 30 min before letting it cool to ambient temperature. This stock seed solution, with an average diameter of 5 to 10 nm and a plasmon band typically centered at 389 nm, was diluted with nanopure water to 100 mL and stored overnight in the dark at 4 °C to allow the deactivation of unreacted borohydride. Fifteen milliliters of this seed solution was added to a mixture of 75 mL of nanopure water and 2.0 mL of fresh 1 %wt sodium citrate solution brought to a boil in a 250-mL single-neck round bottom flask under reflux and under vigorous stirring using an oil bath at 120 °C. This was followed 30 sec later by the addition of 1.7 mL of fresh 1 %wt $AgNO_3$ and the solution was left to stir for 60 min. At this point in the process, the resulting Ag cores had an average diameter of 20 nm and a plasmon band near 390 nm. The 30-nm silver cores were obtained by adding 1.7 mL of 1 %wt $AgNO_3$ and 2 mL of 1 %wt sodium citrate to this suspension, stirring for an additional 60 min, and repeating this sequence a second time. The plasmon resonance of the resulting 30-nm nanoparticle solution displayed a maximum between 402 and 406 nm. The 45-nm silver cores were prepared using the 20-nm core mixture (diluted to 100 mL beforehand) as starting material using the following procedure: 75 mL of nanopure water and 10 mL of the 20-nm cores were mixed in a clean 250-mL round bottom flask and heated to 88 °C under vigorous stirring. 2.0 mL of 1 %wt sodium citrate was added to the mixture, followed 30 s later by the addition of 1.7 mL of fresh 1 %wt $AgNO_3$. The mixture was left to stir for 2 h, allowed to cool to ambient temperature under moderate stirring, and diluted to 100 mL. The plasmon band of this solution was typically centered between 407 and 410 nm. Finally, the 60- and 75-nm silver cores were synthesized using the 45-nm nanoparticles as starting material: the 60-nm cores were prepared by mixing 50 to 40 mL of nanopure water (30 mL colloid + 60 mL water to prepare the 75-nm core size) and bringing the mixture to a temperature of 85 °C under vigorous stirring, followed by the addition of 2.0 mL 1 %wt sodium citrate and, 30 s later, 1.7 mL 1 %wt $AgNO_3$. All colloid dispersions were kept in the dark at 4 °C before condensation of the silica spacer shell, typically 24 h after their synthesis.

Preparation of Ag@SiO_2 Core-Shell Nanoparticles

In order to minimize the partial dissolution of silver by the ammonia used in conventional Stöber sol-gel procedures [49], the condensation of silica shells on our metallic colloids was performed using an ammonia-free synthesis route adapted from the literature [50]. In a 50-mL polypropylene conical tube, 0.20 to 0.85 mL (depending on the desired shell thickness) of a 9-mM TEOS solution in ethanol was mixed with 20 mL of anhydrous ethanol. 2.5 mL of Ag NPs dispersion in water and 0.25 mL of 40 % dimethylamine were added to the TEOS solution before sealing and stirring during 20–24 h. The resulting Ag@SiO_2 core-shell NPs were centrifuged at speeds and durations optimized for each colloid size: 15 min at 12,000 RCF for the 30-nm NPs, 15 min at 10,000 RCF (45 nm), 10 min at 10,000 RCF (60 nm) or 10 min at 8000 RCF (75 nm). For the present study, each Ag@SiO_2 population with a given core size and shell thickness was prepared in triplicate, then pooled and diluted with ethanol to an optical density of 1.0 (see Figures S1 and Table S1, Supplementary Material†).

Fluorescent Labeling of Ag@SiO_2 Core-Shell Nanoparticles

Condensation of an outer thin silica shell incorporating fluorescent silane moieties on the Ag@SiO_2 NPs was done using a procedure adapted from our previous work [39]. The fluorescent dyes used in the present study were commercially available isothiocyanate-functionalized organic fluorophores reacted with aminopropyltriethoxysilane (APS) using the following protocol: 23 μmoles of fluorophore was weighted (8.8 mg for FiTC, 16.0 mg for EiTC, 12.2 mg for RBiTC) and dissolved in 450 μL of anhydrous DMF. 6.4 μL of APS and 6.4 μL of triethylamine were added and the resulting mixture was left to react in the dark at room temperature for 3 h. The APS-modified fluorophore solution was diluted to 50 mL with anhydrous ethanol and stored in the dark at -20 °C until use (within 1 week after their preparation). In preparation for the condensation procedure, the actual nanoparticle concentration of the different Ag@SiO_2 samples was determined by dissolving the cores and determining the silver content by inductively coupled plasma atomic emission spectrometry (ICP-AES) combined with the estimation of the average spherical core volume by TEM (see Supplementary Material† for details). Using this information, the concentration of each core-shell aliquot was adjusted to provide a total available silica surface of 4×10^{13} nm^2/mL for the deposition of the outer silica layer, assuming an identical reactivity of the surface siloxane groups towards the silane coupling agent (independently of core size or shell thickness). Stöber condensation of the outer fluorescent silica shells on the Ag@SiO_2 NPs was achieved in triplicate in 2 mL polypropylene vials by addition, in sequence, of 1.50 mL of the normalized Ag@SiO_2 NP suspension in ethanol, 5.0 μL of the APS-derivatized fluorophore solution (0.46 mM), 45 μL of the 9-mM TEOS solution in ethanol, and 18 μL of aqueous ammonia. The vials were inserted in a 24-slot thermomixer (Model

Thermomixer C, Eppendorf) and the reaction was allowed to proceed for 16–20 h at 20 °C and stirring at 800 rpm. The resulting fluorescent nanoparticles were purified by three consecutive centrifugations and finally dispersed in 800 μL of ethanol. The thickness of the fluorescent outer shell was estimated at (1.0 ± 0.2) nm from TEM images and incorporation yields were calculated (see Supplementary Material† for details).

Characterization

Nanoparticles were characterized by UV-visible spectrophotometry (Model Cary 50, Agilent Technologies), inductively coupled plasma atomic emission spectrometry or ICP-AES (Model Optima 3000, Perkin Elmer), transmission electronic microscopy or TEM (Model Tecnai G2 Spirit, FEI), spectrofluorimetry (Model Fluorolog 3, Jobin-Yvon Horiba), and time-correlated single photon counting time-resolved fluorimetry or TCSPC (Model FluoTime 200, PicoQuant GmbH). Fluorescence decay curves were fitted with a two-exponential model with reconvolution of the instrumental response function (FluoFit data analysis software, PicoQuant GmbH).

Results and Discussion

Absorption Spectra of Ag@SiO_2 Nanoarchitectures

Four distinct Ag nanoparticles populations with diameters of (27 ± 4) nm, (40 ± 5) nm, (60 ± 8) nm, and (74 ± 10) nm were synthesized for this study (Fig. 1). Because of changes in absorption and scattering efficiencies and in the local intensity of the plasmon-generated local electric field, these silver colloids are expected to interact with light differently. Mie theory predicts that particles smaller than ~30 nm support plasmonic oscillations of reduced amplitude and show a characteristic extinction dominated by absorptive phenomena, while larger particles are more efficient at scattering light [51]. Extinction cross-section values measured for the four core sizes vary accordingly, from (2.62 ± 0.02) × 10^7 nm^2 for 27-nm nanoparticles to (19.8 ± 0.3) × 10^7 nm^2 for the 74-nm nanoparticles (see Table S1 in Supplementary Material†). The extent of the plasmon-enhanced electric field into the surrounding media was evaluated by comparing the wavelength shift of the plasmon band for silver cores of various sizes coated with silica shell of varying thickness and dispersed in ethanol (Fig. 2). The results show that the red-shift of the plasmon band increases with spacer thickness until the oscillating electric field is completely confined in the silica shell, at which point the maximal wavelength becomes constant. This study also shows, albeit indirectly, how the plasmon-enhanced electric field extends to a greater distance from larger silver cores, i.e., ~10 nm for 27-nm cores and over 25 nm for 75-nm cores (Fig. 2C). These experimental values are of particular interest for the design of multilayer concentric core-shell architectures and for controlling the range of LSPR sensing by adjusting the size of the metallic domains and the thickness of the dielectric shells.

Influence of Metal Core Size and Spacer Shell Thickness

Ag@SiO_2 core-shell nanoparticles with various core diameters and space shell thicknesses were coated with a thin layer of fluorescein—a high quantum yield (95 % at pH > 8) fluorescent dye frequently used as a probe for MEF studies [52]—and their fluorescence intensity was compared as a function of core diameter and spacer shell thickness. The concentration of nanoparticles in each sample was adjusted to contain the same amount of fluorescein molecules incorporated in the outer silica layer (see Supplementary Material†) and care was taken to keep the optical density below 0.05 at the plasmon and fluorescence excitation wavelengths in order to minimize scattering and inner-filter effects. The results, shown in Fig. 3, mirror the plasmonic field range values extrapolated from the extinction measurements shown in Fig. 2, i.e., smaller cores support a weaker plasmon and only enhance the emission of fluorophores located closer from the metal surface (less than 10 nm away from the 27-nm cores). Interestingly, we observed that signal intensity values reach the same maximum values (within experimental error) at the same distance from the core (~5 nm) for all nanoparticle core diameters except for the smaller ones. This result confirms a previous study performed

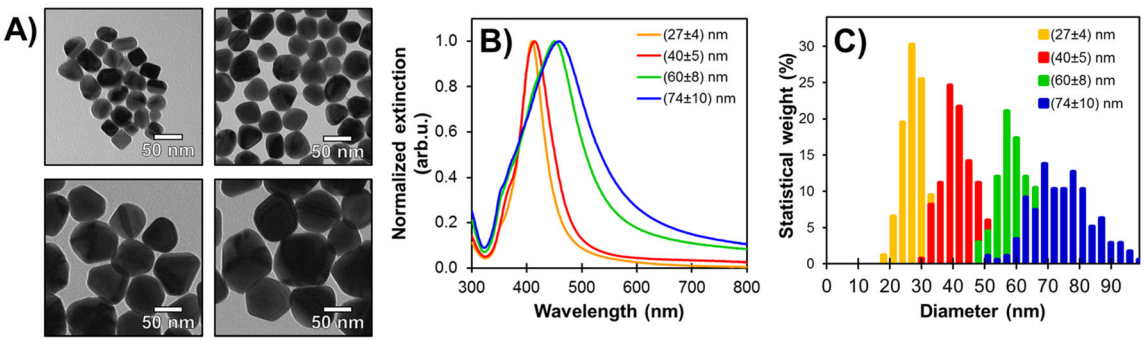

Fig. 1 **a** Representative transmission electron micrographs. **b** UV-VIS extinction spectra in H_2O. **c** Size distribution histograms (C, $N > 150$, 3-nm bins) of Ag cores after seed-growth synthesis

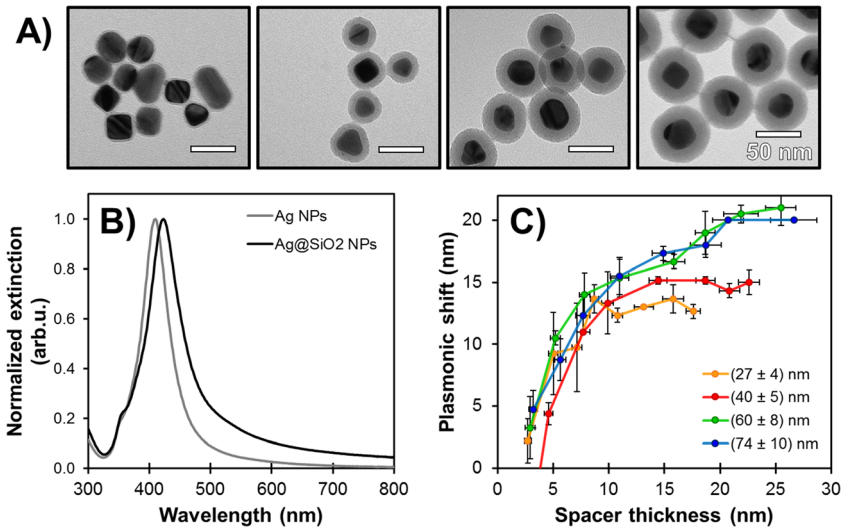

Fig. 2 **a** Transmission electronic micrographs of (27 ± 4) nm Ag cores coated with silica shells (2.7 ± 0.3), (7.1 ± 0.4), (13.1 ± 0.9), and (17.6 ± 0.6) nm in thickness, respectively. **b** Comparison of extinction spectra for 27-nm Ag cores and Ag@SiO_2 NPs with 15-nm thick coating dispersed in ethanol. **c** Plasmonic shift as a function of shell thickness for different core sizes

on silver island films [27] in which the MEF enhancement was reported to be relatively constant, at a distance of ~8 nm from the core, for silver particle diameters in the 40- to 70-nm range. As a consequence, a majority of the fluorescence signal originates from a region 5-10 nm from the metal surface for the 45-nm cores (5–15 nm for the 60- and 75-nm cores).

Since the enhancement of fluorescence close to a metallic surface is known to be accompanied by a decrease in the lifetime of excited states, fluorescence lifetime measurements are a useful indicator of MEF. Fluorescence decay curves were acquired for Ag@SiO_2@SiO_2 + FiTC core-shell NPs as a function of core size and distance from the core to the outer fluorescent layer, and the results (Fig. 4 and Table S2 in Supplementary Material[†] for complete lifetime data) show fluorescence lifetime values increasing with distance from the core for all core diameters. The shorter range of the plasmon from the 27-nm cores hypothesized from Fig. 3 can be observed in the fluorescence lifetime values which seem to plateau when the fluorescent layer is positioned beyond 10 nm from the core surface. The independence of fluorescence enhancement on core size for 60- and 75-nm cores observed on Fig. 3 is confirmed by very similar excited state lifetimes for all spacer shell thickness values of the two core-shell nanostructures. Interestingly, the fluorescence lifetime values measured for the thicker spacers remain inferior to the value of 3.03 ns measured for FiTC in solid silica nanoparticles (SiO_2@SiO_2 + FiTC), an indication that the influence of the core plasmon extends beyond the silica shells investigated in this work.

Quantification of Enhancement Factor (EF)

Formalisms were developed previously for the determination of fluorescence enhancement factors (EF) for various systems including single molecules in bowtie nanoantennas [25] and silica-coated silver island films [24]. In the case of freely diffusing MEF-capable core-shell nanostructures, the development of a generalized methodology for the determination of EFs is hindered by the propensity of colloidal suspensions to

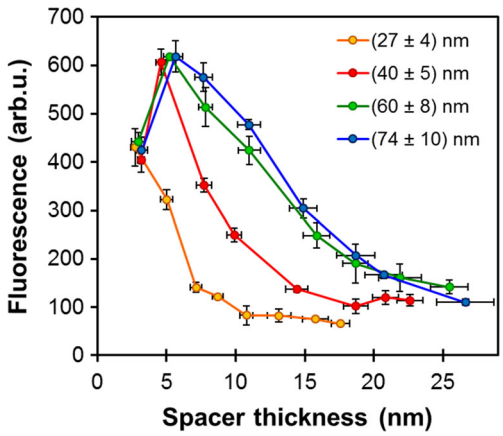

Fig. 3 Fluorescence intensity for Ag@SiO_2@SiO_2 + FiTC (λ_{exc} = 485 nm, λ_{em} = 520 nm) with varying core sizes and silica spacer thickness (N = 3)

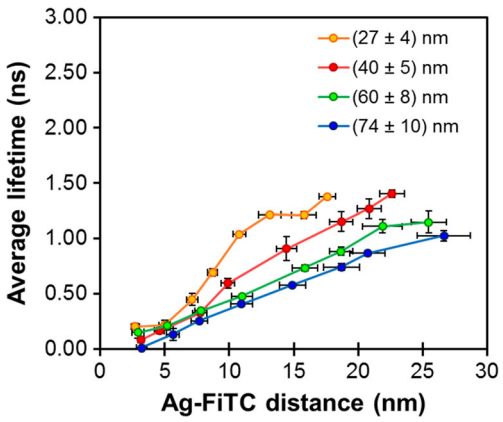

Fig. 4 Average fluorescence lifetimes for Ag@SiO_2@SiO_2 + FiTC with varying core sizes and silica spacer thickness (two-exponential model with IRF deconvolution using non-fluorescent Ag@SiO_2 NPs suspended in ethanol; N = 3)

aggregate and change with time; consequently, various strategies were devised by research groups to determine EFs for their particular systems [30, 36, 39, 53, 54].

The EF in core-shell systems is generally defined as F_{NP}/F_0, where F_{NP} is the emission intensity measured from a certain number of fluorescent molecules in the vicinity of plasmonic cores, and F_0 is that measured from an equal number of emitters without enhancement. Most of the discrepancy in EF values in literature comes from the difficulty of measuring F_0 in conditions comparable to F_{NP} [53]. For example, Tovmachenko et al. [55] and Lin et al. [56] used silica nanoparticles coated with fluorescent molecules as a reference; a disadvantage to this approach is the difficulty to accurately quantify the concentration of silica NPs used to estimate F_0. Another method involves dissolving the metal cores with chloride or cyanide ions, nitric acid, or hydrogen peroxide and measuring the intrinsic signal of the remaining nanoshells [30, 36, 39]. However, this process may take from a few hours to a few days to complete depending on the oxidant used and the porosity of the silica shell, during which time nanoparticle aggregation and sedimentation can occur. Purification of the nanoshells by centrifugation may also induce losses, which will result in overestimated EF values.

The method used in the present work assumes an identical number of molecular emitters generating F_{NP} and F_0 in the probed volume and requires that the concentration of fluorophore and nanoparticles be chosen so that inner-filter effects are minimized. As such, we calculated EF as the ratio of the raw fluorescence measured in core-shell suspensions by the signal of the incorporated molecules ($F_{incorporated}$). However, this value is impossible to quantify directly: we chose to subtract the signal of the supernatant after condensation of the fluorescent outer shell ($F_{residual}$) from a reaction blank (F_{total}, see Supplementary Material†) in otherwise similar conditions of solvent, pH, etc.:

$$EF = \frac{F_{NP}}{F_0} = \frac{F_{NP}}{F_{incorporated}} = \frac{F_{NP}}{F_{total} - F_{residual}}$$

Figure 5a shows the EF for the $Ag@SiO_2@SiO_2$ + FiTC system as a function of core size and spacer shell thickness calculated from the intensity readings of Fig. 3. The maximum EF values of ~10 obtained for fluorescein ~5 nm away from cores 40–75 nm in diameter are similar to values measured in similar core-shell nanostructures by the core dissolution method [57, 58]. The region within 5 nm from the core is presumably dominated by quenching effects, while fluorescent molecules 15 nm or more from the core are largely beyond the reach of the plasmon. These values could be useful as guidelines for the design of simpler, spacer-less core-shell nanoparticles, knowing that fluorescent coatings thicker than 10–15 nm will not improve signal enhancements significantly [35, 59].

Enhancement factors were also determined by the same method for $Ag@SiO_2@SiO_2$ + dye core-shell nanoparticles prepared with two other fluorophores with different quantum yields and degrees of spectral overlap with the core plasmonic band. Fluorescein, eosin, and rhodamine B are xanthene dyes with similar quantum yields (0.95, 0.70, and 0.95, respectively) and excited state lifetimes (3.9, 2.8, and 2.5 ns, respectively) in ethanol. However, the degree of overlap of their excitation-emission spectra with the plasmon band varies considerably, i.e., excitation bands are centered at 490, 530, and 550 nm for FiTC, EiTC, and RBiTC, respectively (Figure S5, Supplementary Material†). Figure 5b shows the enhancement factors measured for FiTC, EiTC, and RBiTC as a function of spacer thickness for 75-nm cores. There is a clear dependence on the overlap of the plasmonic band (maximum at 460 nm) with the fluorophores' excitation band: EF values for ~5-nm spacers decrease from 10.9 (FiTC), to 4.9 (EiTC) to 3.5 (RBiTC). For smaller particles with a blue-shifted extinction, this relation becomes especially apparent with the loss of good overlap for RBiTC (Figure S6 in Supplementary Material†). Since Mie theory predicts that the increase of the plasmonic core size induces a higher efficiency and a notable red-shift of the scattering mode, a dipole-dipole interaction for 60- and 75-nm cores can be achieved with EiTC and RBiTC: in comparison, this coupling is lost for absorption-dominated 27- and 40-nm silver cores. Interestingly, Fig. 5b also demonstrates that the optimal distance for maximal EF is identical for all fluorophores with sufficient overlap. Therefore, in these conditions, MEF can be used to investigate plasmonic properties

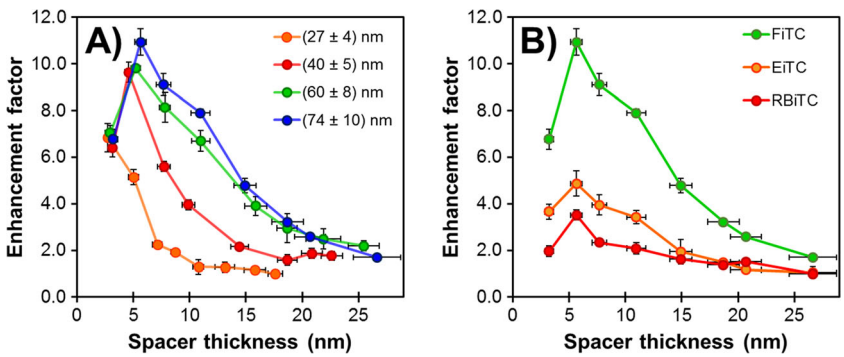

Fig. 5 **a** Fluorescence enhancement factors (EF) for $Ag@SiO_2@SiO_2$ + FiTC (λ_{exc} = 485 nm, λ_{em} = 520 nm) with varying core sizes and silica spacer thickness (N = 3). **b** Enhancement factors for 74-nm cores with different xanthene fluorophores and silica spacer thickness

in core-shell nanostructures and improve their design to incorporate sensitive fluorescent molecules of interest.

Summary and Conclusion

In this paper, we have used $Ag@SiO_2@SiO_2$ + fluorophore NPs with well-controlled geometry as tunable systems to study metal-enhanced fluorescence with regard to the position of molecules in the plasmon-induced electric field, the degree of spectral overlap with different fluorophores, and the size of the metallic nano-domain. The combination of steady-state and time-resolved measurements has allowed to identify optimal values for key parameters in the design of colloidal MEF sensors: (1) Metallic particles with low absorptive and high scattering efficiencies—e.g., larger silver NPs up to 75 nm—offer a better plasmonic range to induce dipole-dipole interactions with neighboring fluorophores; (2) Maximum enhancement of fluorescence is observed between 10 and 15 nm from the metal surface, whereas quenching phenomena are dominant 5 nm or less from the core; (3) For silver cores, MEF is highly dependant on the degree of spectral overlap with fluorophores. Our experiments involved three available commercial fluorophores (fluorescein, eosin, rhodamine B), but we believe the methodology and conclusions of the study could be extended to other nanoparticle compositions. Because many labeling molecules in biology and biochemistry have fluorescence properties in this region of the visible spectra (450–600 nm), we believe our conclusions on the optimal distance in plasmonic core-shell architectures could be generalized and applied in future generation of MEF-enabled probes.

Acknowledgments This work was supported by the Natural Sciences and Engineering Research Council of Canada, the "Fonds de la Recherche du Québec – Nature et Technologies" and the Canadian Foundation for Innovation. The authors would also like to thank Félix-Antoine Lavoie, Samuel Ouellet, and Cyril Caron for insightful discussions about fluorescence spectroscopy and lifetime experiments.

References

1. Ranasinghe RT, Brown T (2005) Fluorescence based strategies for genetic analysis. Chem Commun 44:5487–5502
2. Dressler C, Beuthan J, Mueller G, Zabarylo U, Minet O (2006) Fluorescence imaging of heat-stress induced mitochondrial long-term depolarization in breast cancer cells. J Fluoresc 16(5):689–695
3. Zhang M, Yu M, Li F, Zhu M, Li M, Gao Y, Li L, Liu Z, Zhang J, Zhang D, Yi T, Huang C (2007) A highly selective fluorescence turn-on sensor for cysteine/homocysteine and its application in bioimaging. J Am Chem Soc 129(34):10322–10323
4. Telford WG, Hawley T, Subach F, Verkhusha V, Hawley RG (2012) Flow cytometry of fluorescent proteins. Methods 57(3):318–330
5. Guo K, Achilefu S, Berezin MY (2012) Dating bloodstains with fluorescence lifetime measurements. Chemistry 18(5):1303–1305
6. Frascione N, Gooch J, Daniel B (2013) Enabling fluorescent biosensors for the forensic identification of body fluids. Analyst (Cambridge, U K) 138(24):7279–7288
7. Loutfy RO, Aroca R (1982) Interaction of indium metal with phthalocyanine molecules: luminescence enhancement. J Lumin 26(4): 359–366
8. Wokaun A, Lutz HP, King AP, Wild UP, Ernst RR (1983) Energy transfer in surface enhanced luminescence. J Chem Phys 79(1):509
9. Lakowicz JR (2001) Radiative decay engineering: biophysical and biomedical applications. Anal Biochem 298(1):1–24
10. Geddes CD, Lakowicz JR (2002) Metal-induced fluorescence: editorial. J Fluoresc 12(2):121–129
11. Kamat PV (2002) Photophysical, photochemical and photocatalytic aspects of metal nanoparticles. J Phys Chem B 106(32):7729–7744
12. Aslan K, Gryczynski I, Malicka J, Matveeva E, Lakowicz JR, Geddes CD (2005) Metal-enhanced fluorescence: an emerging tool in biotechnology. Curr Opin Biotech 16(1):55–62
13. Anger P, Bharadwaj P, Novotny L (2006) Enhancement and quenching of single-molecule fluorescence. Phys Rev Lett 96(11): 113002
14. Geddes CD (2013) Metal-enhanced fluorescence. Phys Chem Chem Phys 15(45):19537
15. Fort E, Grésillon S (2008) Surface enhanced fluorescence. J Phys D: Appl Phys 41(1):013001
16. Lakowicz JR, Ray K, Chowdhury M, Szmacinski H, Fu Y, Zhang J, Nowaczyk K (2008) Plasmon-controlled fluorescence: a new paradigm in fluorescence spectroscopy. Analyst (Cambridge, U K) 133(10):1308–1346
17. Guerrero AR, Aroca RF (2011) Surface-enhanced fluorescence with shell-isolated nanoparticles (SHINEF). Angew Chem Int Ed 50(3):665–668
18. Darvill D, Centeno A, Xie F (2013) Plasmonic fluorescence enhancement by metal nanostructures: shaping the future of bionanotechnology. Phys Chem Chem Phys 15(38):15709–15726
19. Zhang B, Kumar RB, Dai H, Feldman BJ (2014) A plasmonic chip for biomarker discovery and diagnosis of type 1 diabetes. Nat Med 20(8):948–953
20. Deng W, Xie F, Baltar HT, Goldys EM (2013) Metal-enhanced fluorescence in the life sciences: here, now and beyond. Phys Chem Chem Phys 15(38):15695–15708
21. Ayala-Orozco C, Urban C, Knight MW, Urban AS, Neumann O, Bishnoi SW, Mukherjee S, Goodman AM, Charron H, Mitchell T, Shea M, Roy R, Nanda S, Schiff R, Halas NJ, Joshi A (2014) Au nanomatryoshkas as efficient near-infrared photothermal transducers for cancer treatment: benchmarking against nanoshells. ACS Nano 8(6):6372–6381
22. Ray K, Badugu R, Lakowicz JR (2007) Polyelectrolyte layer-by-layer assembly to control the distance between fluorophores and plasmonic nanostructures. Chem Mater 19(24):5902–5909
23. Dragan AI, Bishop ES, Casas-Finet JR, Strouse RJ, McGivney J, Schenerman MA, Geddes CD (2012) Distance dependence of metal-enhanced fluorescence. Plasmonics 7(4):739–744
24. Mishra H, Mali BL, Karolin J, Dragan AI, Geddes CD (2013) Experimental and theoretical study of the distance dependence of metal-enhanced fluorescence, phosphorescence and delayed fluorescence in a single system. Phys Chem Chem Phys 15(45):19538–19544
25. Kinkhabwala A, Yu Z, Fan S, Avlasevich Y, Müllen K, Moerner WE (2009) Large single-molecule fluorescence enhancements produced by a bowtie nanoantenna. Nat Photonics 3(11):654–657
26. Taylor RW, Lee TC, Scherman OA, Esteban R, Aizpurua J, Huang FM, Baumberg JJ, Mahajan S (2011) Precise subnanometer plasmonic junctions for SERS within gold nanoparticle assemblies using cucurbit[n]uril "glue". ACS Nano 5(5):3878–3887

27. Zhang J, Fu Y, Chowdhury MH, Lakowicz JR (2007) Single-molecule studies on fluorescently labeled silver particles: effects of particle size. J Phys Chem C 112(1):18
28. Bardhan R, Grady NK, Halas NJ (2008) Nanoscale control of near-infrared fluorescence enhancement using Au nanoshells. Small 4(10):1716–1722
29. Bardhan R, Grady NK, Cole JR, Joshi A, Halas NJ (2009) Fluorescence enhancement by Au nanostructures: nanoshells and nanorods. ACS Nano 3(3):744–752
30. Magnan F, Gagnon J, Fontaine FG, Boudreau D (2013) Indium@silica core-shell nanoparticles as plasmonic enhancers of molecular luminescence in the UV region. Chem Commun 49(81): 9299–9301
31. Ayala-Orozco C, Liu JG, Knight MW, Wang Y, Day JK, Nordlander P, Halas NJ (2014) Fluorescence enhancement of molecules inside a gold nanomatryoshka. Nano Lett 14(5):2926–2933
32. Zhang J, Fu Y, Chowdhury MH, Lakowicz JR (2007) Metal-enhanced single-molecule fluorescence on silver particle monomer and dimer: coupling effect between metal particles. Nano Lett 7(7): 2101–2107
33. Malicka J, Gryczynski I, Gryczynski Z, Lakowicz JR (2003) Effects of fluorophore-to-silver distance on the emission of cyanine–dye-labeled oligonucleotides. Anal Biochem 315(1):57–66
34. Chen Y, Munechika K, Ginger DS (2007) Dependence of fluorescence intensity on the spectral overlap between fluorophores and plasmon resonant single silver nanoparticles. Nano Lett 7(3):690–696
35. Brouard D, Ratelle O, Perreault J, Boudreau D, St-Louis M (2015) PCR-free blood group genotyping using a nanobiosensor. Vox Sang 108(2):197–204
36. Aslan K, Wu M, Lakowicz JR, Geddes CD (2007) Fluorescent core-shell Ag@SiO2 nanocomposites for metal-enhanced fluorescence and single nanoparticle sensing platforms. J Am Chem Soc 129(6):1524–1525
37. Brouard D, Viger ML, Bracamonte AG, Boudreau D (2011) Label-free biosensing based on multilayer fluorescent nanocomposites and a cationic polymeric transducer. ACS Nano 5(3):1888–1896
38. Tam F, Goodrich GP, Johnson BR, Halas NJ (2007) Plasmonic enhancement of molecular fluorescence. Nano Lett 7(2):496–501
39. Lessard-Viger M, Rioux M, Rainville L, Boudreau D (2009) FRET enhancement in multilayer core-shell nanoparticles. Nano Lett 9(8): 3066–3071
40. Reineck P, Gomez D, Ng SH, Karg M, Bell T, Mulvaney P, Bach U (2013) Distance and wavelength dependent quenching of molecular fluorescence by Au@SiO2 core-shell nanoparticles. ACS Nano 7(8):6636–6648
41. Pyatenko A, Yamagushi M, Suzuki M (2007) Synthesis of spherical silver nanoparticles with controllable sizes in aqueous solutions. J Phys Chem C 111(22):7910–7917
42. Rycenga M, Cobley CM, Zeng J, Li W, Moran CH, Zhang Q, Qin D, Xia Y (2011) Controlling the synthesis and assembly of silver nanostructures for plasmonic applications. Chem Rev 111(6):3669–3712
43. Wuithschick M, Birnbaum A, Witte S, Sztucki M, Vainio U, Pinna N, Rademann K, Emmerling F, Kraehnert R, Polte J (2015) Turkevich in new robes: key questions answered for the most common gold nanoparticle synthesis. ACS Nano 9(7):7052–7071
44. McClain MJ, Schlather AE, Ringe E, King NS, Liu L, Manjavacas A, Knight MW, Kumar I, Whitmire KH, Everitt HO, Nordlander P, Halas NJ (2015) Aluminum nanocrystals. Nano Lett 15(4):2751–2755
45. Shiomi S, Kawamori M, Yagi S, Matsubara E (2015) One-pot synthesis of silica-coated copper nanoparticles with high chemical and thermal stability. J Colloid Interface Sci 460:47–54
46. Li H, Xia H, Wang D, Tao X (2013) Simple synthesis of monodisperse, quasi-spherical, citrate-stabilized silver nanocrystals in water. Langmuir 29(16):5074–5079
47. Wan Y, Guo Z, Jiang X, Fang K, Lu X, Zhang Y, Gu N (2013) Quasi-spherical silver nanoparticles: Aqueous synthesis and size control by the seed-mediated Lee–Meisel method. J Colloid Interface Sci 394:263–268
48. Bastús NG, Merkoçi F, Piella J, Puntes V (2014) Synthesis of highly monodisperse citrate-stabilized silver nanoparticles of up to 200 nm: kinetic control and catalytic properties. Chem Mater 26(9): 2836–2846
49. Stöber W, Fink A, Bohn E (1968) Controlled growth of monodisperse silica spheres in the micron size range. J Colloid Interface Sci 26(1):62–69
50. Kobayashi Y, Katakami H, Mine E, Nagao D, Konno M, Liz-Marzan LM (2005) Silica coating of silver nanoparticles using a modified Stober method. J Colloid Interface Sci 283(2):392–396
51. Evanoff DD, Chumanov G (2004) Size-controlled synthesis of nanoparticles. 2. Measurement of extinction, scattering, and absorption cross sections. J Phys Chem B 108(37):13957–13962
52. Lakowicz JR, Shen Y, D'Auria S, Malicka J, Fang J, Gryczynski Z, Gryczynski I (2002) Radiative decay engineering. 2. Effects of Silver Island films on fluorescence intensity, lifetimes, and resonance energy transfer. Anal Biochem 301(2):261–277
53. Guerrero AR, Zhang Y, Aroca RF (2012) Experimental confirmation of local field enhancement determining far-field measurements with shell-isolated silver nanoparticles. Small 8(19):2964–2967
54. Zhang D, Nettles CB (2015) A generalized model on the effects of nanoparticles on fluorophore fluorescence in solution. J Phys Chem C 119(14):7941–7948
55. Tovmachenko OG, Graf C, van den Heuvel DJ, van Blaaderen A, Gerritsen HC (2006) Fluorescence enhancement by metal-core/silica-shell nanoparticles. Adv Mater 18(1):91–95
56. Lin H-H, Chen IC (2015) Study of the interaction between gold nanoparticles and Rose Bengal fluorophores with silica spacers by time-resolved fluorescence spectroscopy. J Phys Chem C.
57. Asselin J, Roy C, Boudreau D, Messaddeq Y, Bouchareb R, Mathieu P (2014) Supported core-shell nanobiosensors for quantitative fluorescence imaging of extracellular pH. Chem Commun 50(89):13746–13749
58. L-Viger M, Brouard D, Boudreau D (2011) Plasmon-enhanced resonance energy transfer from a conjugated polymer to fluorescent multilayer core − shell nanoparticles: a photophysical study. J Phys Chem C 115(7):2974–2981
59. Viger ML, Live LS, Therrien OD, Boudreau D (2008) Reduction of self-quenching in fluorescent silica-coated silver nanoparticles. Plasmonics 3(1):33–40